

# AIR ENTRAINMENT AND TURBULENCE IN HYDRAULIC JUMPS: FREE-SURFACE FLUCTUATIONS AND INTEGRAL TURBULENT SCALES

G. Zhang<sup>1</sup>, H. Wang<sup>1</sup> and H. Chanson<sup>1</sup>

<sup>1</sup>University of Queensland, School of Civil Engineering, Brisbane QLD 4072, Australia,  
h.chanson@uq.edu.au

**Abstract:** An open channel flow can change from a supercritical to subcritical flow with a strong dissipative process: a hydraulic jump. Herein some new measurements of free-surface fluctuations next to the jump toe and integral turbulent scales in the roller are presented with a focus on turbulent hydraulic jumps with a marked roller. The results highlighted the fluctuating nature of the impingement perimeter in terms of both longitudinal and transverse locations. The air-water flow measurements highlighted the intense flow aeration. The turbulent velocity distributions presented a shape similar to a wall jet solution, and the integral turbulent length scale distributions exhibited a monotonic increase with increasing vertical elevation within  $0.2 < L_z/d_1 < 0.8$  in the shear layer, where  $L_z$  is the integral turbulent length scale and  $d_1$  the inflow depth.

**Keywords:** hydraulic jumps, air entrainment, turbulence free-surface fluctuations, jump toe, integral turbulent time and length scales, physical measurements.

## INTRODUCTION

In an open channel, the transition from supercritical to subcritical flow is characterised by a strong dissipative mechanism, called a hydraulic jump (Fig. 1). The hydraulic jump is an extremely turbulent flow associated with the development of large-scale turbulence, energy dissipation and air entrainment. Some key features in prototype structures include the intense turbulence associated with large jump toe fluctuations, together with the air entrapment at the jump toe and roller aeration, for example seen in Figure 1. Reviews into hydraulic jump research include Rajaratnam (1967), Hager (1992), Chanson (2009,2011) and Murzyn (2010).

This paper presents some new physical experiments performed in a relatively large physical facility. The focus is on the jump toe and its fluctuating shape, and the turbulence in the marked roller. The results emphasise the complicated nature of hydraulic jump flow motion and turbulence characteristics.

## EXPERIMENTAL CHANNEL AND METROLOGY

### Presentation

The experiments were performed in a horizontal rectangular flume (Fig. 2). The channel was 3.2 m long and 0.50 m wide with glass sidewalls and PVC invert. The inflow conditions were controlled

by a vertical gate with a semi-circular rounding ( $\varnothing = 0.3$  m) whose opening was fixed at  $h = 0.024$  m. The experimental flow conditions are summarised in Table 1.

The water discharge was measured with a Venturi meter calibrated on-site with an accuracy of  $\pm 2\%$ . The clear-water flow depths were measured using rail mounted point gauges with a 0.25 mm accuracy. The air-water flow properties were measured using either a double-tip conductivity probes ( $\varnothing = 0.35$  mm,  $\Delta x = 7.1$  mm) or an array of two identical single-tip conductivity probe ( $\varnothing = 0.35$  mm) separated by a transverse distance  $\Delta z$ . An air bubble detector (UQ82.518) excited the probes and the output signals are scanned at 20 kHz per sensor for 45 s. The translation of the probes in the direction normal to the channel invert was controlled by a fine adjustment travelling mechanism connected to a Mitutoyo™ digimatic scale unit. Flow visualisations were conducted with high-shutter speed digital still- and video-cameras.



Fig. 1 - Hydraulic jump stilling basin in operation downstream of Paradise dam spillway (Australia) on 30 December 2010 -  $Q = 6,300$  m<sup>3</sup>/s,  $Re = 1.9 \times 10^7$

Table 1 - Experimental flow conditions (Present study)

$d_1$ (m)	$x_1$ (m)	$Fr_1$	$Re$	Instrumentation	Remarks
0.025 to 0.027	0.25, 0.50, 1.0, 1.5	2.8 to 7.5	$3.8 \times 10^4$ to $7.6 \times 10^4$	Video-camera	Series HW2011
0.024 to 0.028	1.0	2.6 to 8.9	$3.6 \times 10^4$ to $1.0 \times 10^5$	Conductivity probes	Series GZ201011

### Air-water flow signal processing

The analysis of probe voltage outputs was based upon a single threshold technique set at 50% of air-water voltage range. A number of air-water flow properties were calculated, including the void fraction  $C$ , the bubble count rate  $F$  defined as the number of bubbles impacting the probe tip per second, and the air chord time distributions where the chord time is defined as the time spent by the bubble on the probe tip. The interfacial velocity  $V$  was calculated using a cross-correlation technique:  $V = \Delta x/T$  where  $\Delta x$  is the longitudinal distance between both tips and  $T$  is the average interfacial travel time between probe sensors (Crowe et al. 1998). The turbulence level  $Tu$  was deduced from the shapes of cross- and auto-correlation functions (Chanson and Carosi 2007).

The analysis of the signal auto-correlation function provided further information on the integral turbulent scales (Chanson 2007, Chanson and Carosi 2007). The integral turbulent length scale was calculated as

$$L_z = \int_{z=0}^{z=z((R_{xz})_{\max}=0)} (R_{xz})_{\max} \times dz \quad (1)$$

where  $z$  is the transverse (separation) distance and  $(R_{xz})_{\max}$  is the maximum normalised cross-correlation function. The integral turbulent time scale was estimated as

$$T_z = \frac{1}{L_z} \times \int_{z=0}^{z=z((R_{xz})_{\max}=0)} (R_{xz})_{\max} \times T_{xz} \times dz \quad (2)$$

where  $T_{xz}$  is the integral cross-correlation time scale for a transverse separation distance  $dz$ .

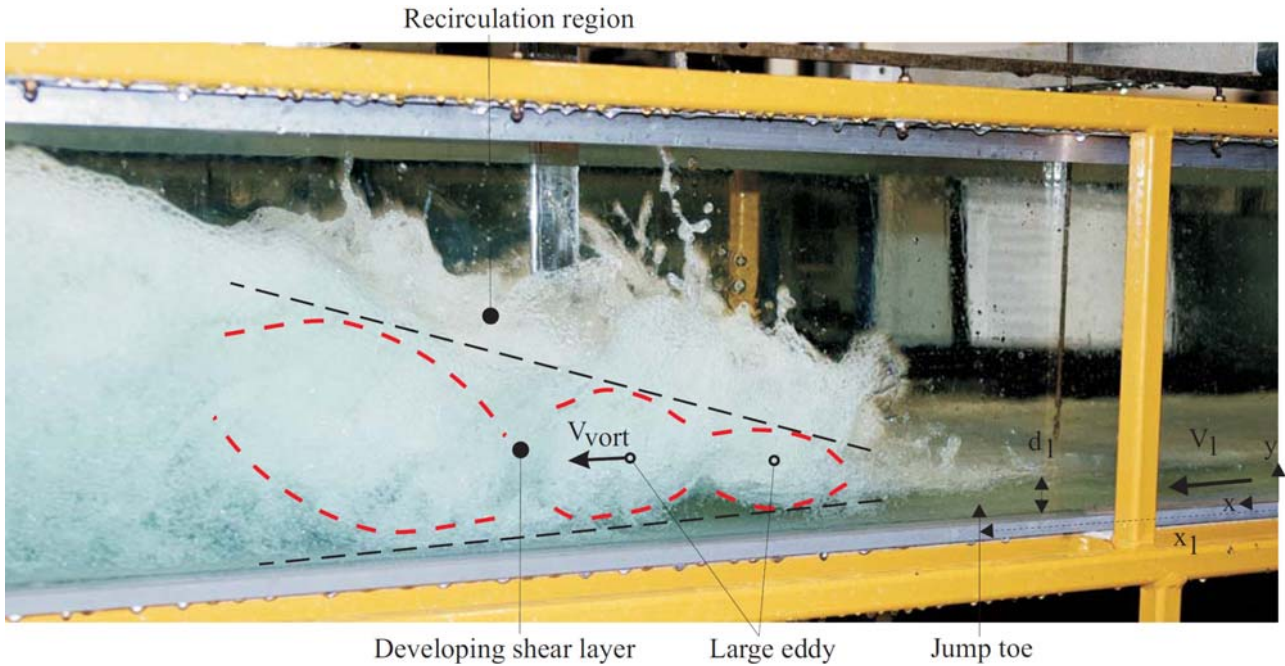


Fig. 2 - Photograph of hydraulic jump experiment: side view with flow from right to left,  $Fr_1 = 6.1$

### BASIC OBSERVATIONS AND JUMP TOE PROPERTIES

For inflow Froude numbers greater than 2 to 3, the hydraulic jump exhibited a marked roller associated with a developing shear layer and large-scale vortical structures (Fig. 2). At the impingement point or jump toe, a flow discontinuity developed and the impingement perimeter shape changed rapidly with time and transverse distance. Figure 3 illustrates some instantaneous impingement perimeter together with the median profile, viewed in elevation. In Figure 3, the arrow shows the main flow direction. Overall the perimeter data suggested the presence of transverse wave patterns with dimensionless wave length  $l_w/W$  between  $2/3$  and  $2$ , where  $W$  is the channel width. The fluctuations in impingement perimeter transverse profile were significant and increased with increasing Froude number, as illustrated in Figure 4.

The longitudinal position of hydraulic jump toe varied with time around a mean position  $x_1$ . The jump toe pulsations were believed to be caused by the growth, advection, and pairing of large-scale vortices in the developing shear layer (Long et al. 1991). Figures 5, 6 and 7 show respectively the jump toe fluctuation frequency, the frequency of ejection of large vortical structures and the advection speed of these large coherent structures. Within the experimental flow conditions, the

data were best correlated by

$$\frac{F_{\text{toe}} \times d_1}{V_1} = 0.054 \times \exp(-0.33 \times Fr_1) \quad (3)$$

$$\frac{F_{\text{vort}} \times d_1}{V_1} = 0.034 \times \exp(-0.26 \times Fr_1) \quad (4)$$

irrespective of the jump toe location  $x_1$ . The present data are compared with Equations (3) and (4) as well as previous results in Figures 5 and 6. The dimensionless advection speed  $V_{\text{vort}}/V_1$  of large-scale coherent structures in the shear layer characterised the convection of large eddies in the mixing layer and it was obtained from digital movie analysis. The data were nearly independent of the inflow conditions and yielded on average  $V_{\text{vort}}/V_1 \approx 0.4$  (Fig. 7).

### AIR-WATER FLOW PROPERTIES

The measurements of void fraction and bubble count rate highlighted two air-water flow regions. Namely, the air-water shear layer and the upper free-surface region (Fig. 2). The developing shear layer was characterised by some strong interactions between entrained air bubbles and vortical structures, associated with a local maximum in void fraction  $C_{\text{max}}$  and a maximum in bubble count rate  $F_{\text{max}}$ . In the shear layer, the distributions of void fractions followed an analytical solution of the advective diffusion equation for air bubbles:

$$C = \frac{Q_{\text{air}}}{Q} \times \left( \exp \left( -\frac{(y'-1)^2}{4 \times D^\#} \right) + \exp \left( -\frac{(y'+1)^2}{4 \times D^\#} \right) \right) \quad (5)$$

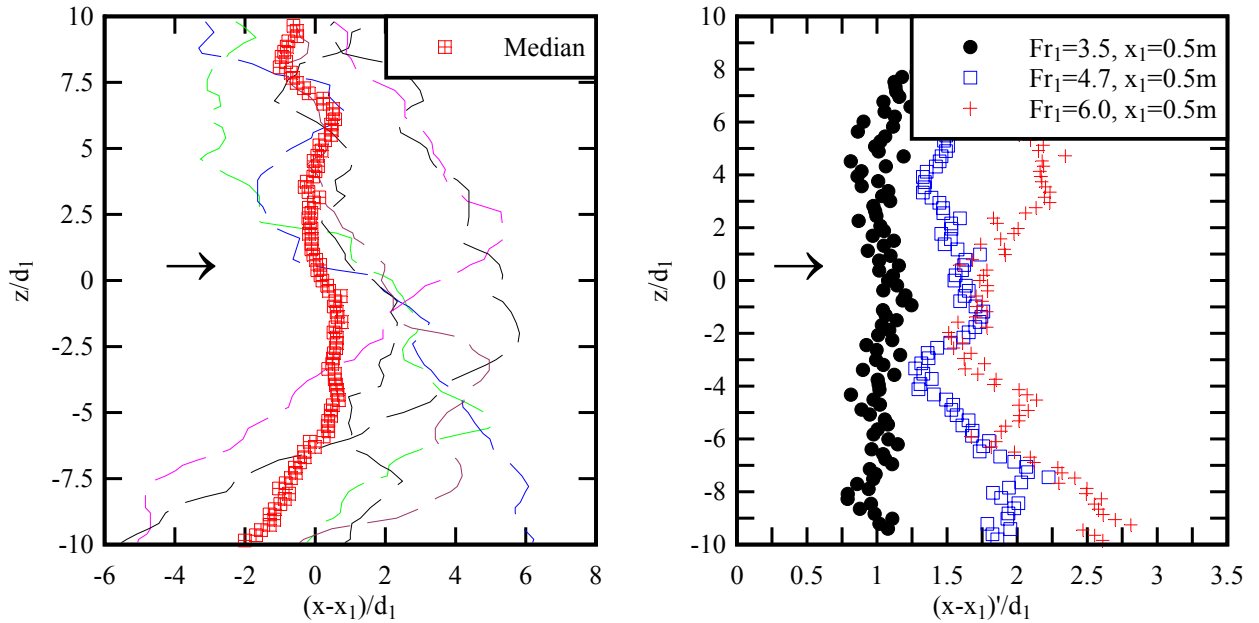


Fig. 3 (Left) - Instantaneous and median impingement perimeter transverse profiles viewed in elevation ( $Fr_1 = 6.0$ ,  $x_1 = 0.5$  m, series HW2011)

Fig. 4 (Right) - Standard deviations of impingement perimeter profile ( $x_1 = 0.5$  m, series HW2011)

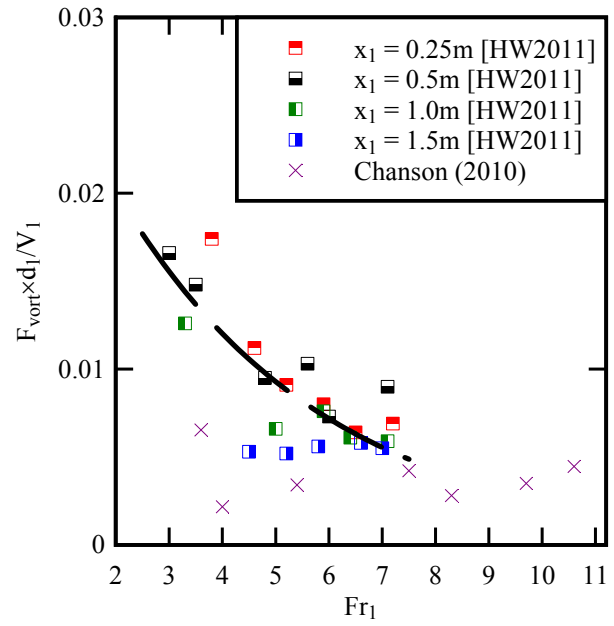
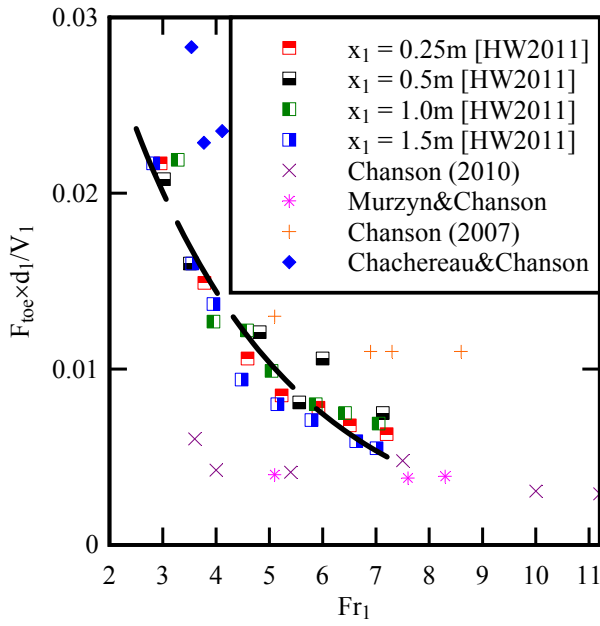


Fig. 5 (Left) - Dimensionless jump toe fluctuation frequency  $F_{toe} \times V_1 / d_1$

Fig. 6 (Right) - Dimensionless frequency of large vortical structure production rate  $F_{vort} \times V_1 / d_1$

where  $Q_{air}$  is the entrained air volume,  $Q$  is the water discharge,  $D^\#$  is a dimensionless air bubble diffusivity,  $X' = X/d_1$ ,  $y' = y/d_1$ ,  $X = x - x_1 + u_r / V_1 \times y$ ,  $u_r$  is the bubble rise velocity (Chanson 2010). In the upper free-surface region above, the void fraction increased monotonically with increasing distance from the invert towards unity. Figure 8 presents some typical vertical distributions of void fraction and bubble count rate.

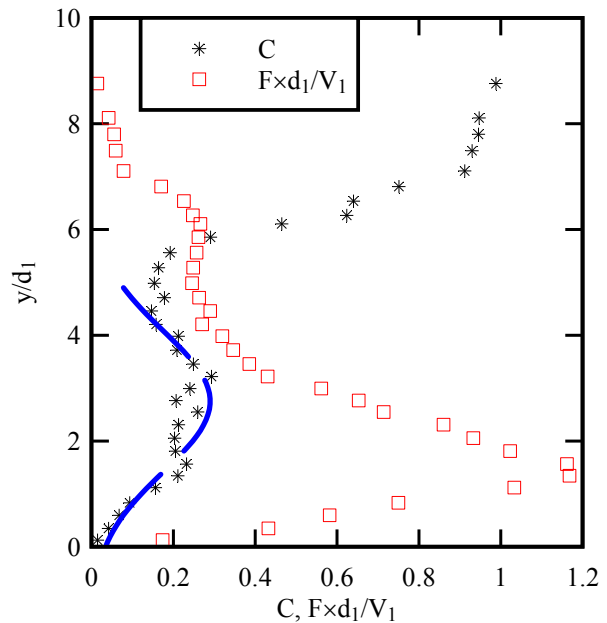
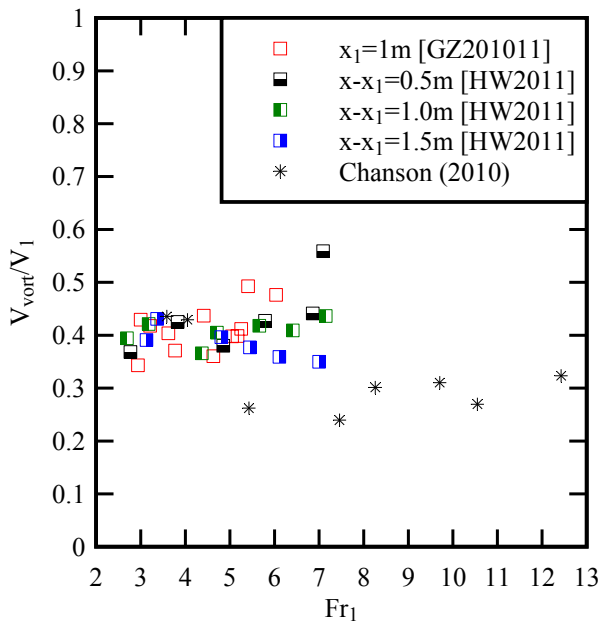


Fig. 7 (Left) - Dimensionless advection speed  $V_{vort} / V_1$  of large-scale vortical structures in the developing shear layer of hydraulic jumps

Fig. 8 (Right) - Dimensionless distributions of void fraction and bubble count rate in hydraulic jump roller ( $Fr_1 = 7.7$ ,  $x - x_1 = 0.30$  m, series GZ201011) - Comparison between void fraction data and Equation (5)

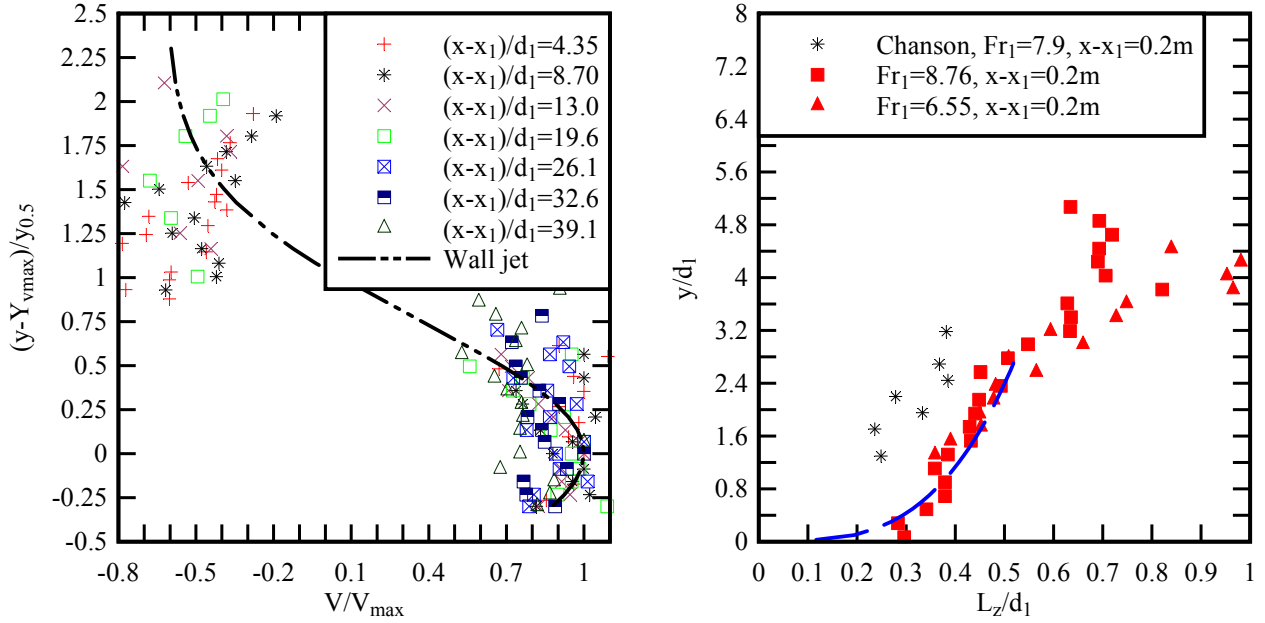


Fig. 9 (Left) - Dimensionless velocity distributions  $V/V_{\max}$  in hydraulic jumps: comparison between experimental data ( $Fr_1 = 8.8$ ,  $d_1 = 0.023$  m,  $x_1 = 1$  m, series GZ201011) and Eq. (7)

Fig. 10 (Right) - Dimensionless distributions of integral turbulent length scale  $L_z/d_1$  in hydraulic jumps at  $x-x_1 = 0.2$  m: comparison between present data (series GZ201011), Chanson's (2007) data and Equation (8)

The interfacial velocity data showed some profiles with a self-similar shape close to wall jet results. Namely, a flow region very close to the bed with a "boundary-layer like" profile where the velocity increases from zero up to a maximum velocity  $V_{\max}$  at  $y = Y_{V_{\max}}$ , and an upper flow region with decreasing velocity with increasing vertical distance. The dimensionless results were best fitted by:

$$\frac{V}{V_{\max}} = \left( \frac{y}{Y_{V_{\max}}} \right)^{\frac{1}{N}} \quad \text{for } \frac{y}{Y_{V_{\max}}} < 1 \quad (6)$$

$$\frac{V - V_{\text{recirc}}}{V_{\max} - V_{\text{recirc}}} = \exp \left( -\frac{1}{2} \times \left[ 1.765 \times \left( \frac{y - Y_{V_{\max}}}{y_{0.5}} \right) \right]^2 \right) \quad \text{for } 1 < \frac{y}{Y_{V_{\max}}} \quad (7)$$

where  $V_{\text{recirc}}$  is the recirculation velocity in the upper free-surface region with  $V_{\text{recirc}} < 0$  typically,  $y_{0.5}$  the vertical elevation where  $V = V_{\max}/2$  and  $N$  is a constant. The present results followed closely the above equations, despite some data scatter, as illustrated in Figure 9 where the data are shown in a self-similar presentation.

Based upon correlation analyses performed on the probe array signal outputs, the integral turbulent length and time scales,  $L_z$  and  $T_z$  respectively, were calculated. Typical results are presented in Figure 10 and compared with an earlier data set. The integral length scale  $L_z$  was closely linked with the sizes of large vortical structures, and the present data indicated that  $0.2 < L_z/d_1 < 0.8$  for a large majority of data independently of Froude number. For  $y/d_1 < 3.5$ , the turbulent length scale data presented a monotonic increase with increasing distance from the invert (Fig. 10). The data

were best correlated by

$$\frac{L_z}{d_1} = \frac{0.6422}{\left(\frac{x-x_1}{d_1}\right)^{0.2411}} \times \left(\frac{y}{d_1}\right)^{0.8624} / \sqrt{(x-x_1)/d_1} \quad \text{for } \frac{y}{d_1} < 4 \quad (8)$$

The distributions of integral turbulent time scales (not shown) showed a decrease with increasing distance from the invert. The results were within  $1.7 < T_z \times (g/d_1)^{0.5} < 4$ .

## CONCLUSION

Detailed physical measurements were conducted in hydraulics jumps with Froude numbers between 2.6 and 8.9, inflow length  $x_1/d_1$  between 10 and 60, and Reynolds numbers up to  $1 \times 10^5$ . The focus of the study was on the impingement properties and on the integral turbulent scales in the roller.

The results highlighted the fluctuating nature of the impingement perimeter, in terms of both longitudinal and transverse directions. The production frequency  $F_{\text{vort}}$  of large coherent structures was very close to the jump toe longitudinal fluctuation frequency  $F_{\text{toe}}$ . The findings emphasised the importance of the impingement perimeter as a source of vorticity. The air-water flow properties highlighted the intense flow aeration with two dominant flow regions: a developing shear layer and a recirculation region above. The turbulent velocity distributions presented a shape similar to a wall jet solution, while the integral turbulent length scale data exhibited a monotonic increase with increasing vertical elevation within  $0.2 < L_z/d_1 < 0.8$  in the shear layer.

The modelling of the air-water mixing zone in turbulent hydraulic jumps remains naive because of the large number of relevant equations to describe the two-phase turbulent flow motion as well as the limited validation data sets. The most successful physical data set were obtained with intrusive phase-detection probes, including this study. A future research direction in hydraulic jump research may see the development of composite models embedding numerical and physical studies.

## ACKNOWLEDGMENTS

The writers thank Ahmed Ibrahim and Jason Van Der Gevel (The University of Queensland) for the technical assistance. The financial support of the Australian Research Council (Grant DP0878922) is acknowledged.

## REFERENCES

- Chachereau, Y., and Chanson, H. (2011). Free-surface fluctuations and turbulence in hydraulic jumps. *Exp. Thermal and Fluid Science*, Vol. 35, No. 6, pp. 896-909 (DOI: 10.1016/j.expthermflusci.2011.01.009).
- Chanson, H. (2007). Bubbly flow structure in hydraulic jump. *European J. of Mech. B/Fluids*, Vol. 26, No. 3, pp.367-384 (DOI:10.1016/j.euromechflu.2006.08.001).
- Chanson, H. (2009). Current knowledge in hydraulic jumps and related phenomena. A survey of experimental results. *European J. of Mech. B/Fluids*, Vol. 28, No. 2, pp. 191-210 (DOI: 10.1016/j.euromechflu.2008.06.004).
- Chanson, H. (2010). Convective transport of air bubbles in strong hydraulic jumps. *Int. J. of Multiphase Flow*, Vol. 36, No. 10, pp. 798-814 (DOI: 10.1016/j.ijmultiphaseflow.2010.05.006).

- Chanson, H. (2011). Hydraulic jumps: Turbulence and air bubble entrainment. *J. La Houille Blanche*, No. 1, pp. 5-16 & Front cover (DOI: 10.1051/lhb/2011026) (ISSN 0018-6368).
- Crowe, C., Sommerfield, M., and Tsuji, Y. (1998). *Multiphase Flows with Droplets and Particles*. CRC Press, Boca Raton, USA, 471 pages.
- Chanson, H., and Carosi, G. (2007). Advanced post-processing and correlation analyses in high-velocity air-water flows. *Env. Fluid Mech.*, Vol. 7, No. 6, pp. 495-508 (DOI 10.1007/s10652-007-9038-3).
- Hager, W.H. (1992). *Energy Dissipators and Hydraulic Jump*. Kluwer Academic Publ., Water Science and Technology Library, Vol. 8, Dordrecht, The Netherlands, 288 pages.
- Long, D., Rajaratnam, N., Steffler, P.M., and Smy, P.R. (1991). Structure of flow in hydraulic jumps. *J. Hyd. Res.*, IAHR, Vol. 29, No. 2, pp. 207-218.
- Murzyn, F. (2010). Assessment of Different Experimental Techniques to Investigate the Hydraulic Jump: Do They Lead to the Same Results? in "Hydraulic Structures: Useful Water Harvesting Systems or Relics?", *Proc. 3<sup>rd</sup> International Junior Researcher and Engineer Workshop on Hydraulic Structures (IJREWHS'10)*, 2-3 May 2010, Edinburgh, Scotland, R. Janssen and H. Chanson (Eds), Hydraulic Model Report CH80/10, School of Civil Engineering, The University of Queensland, Brisbane, Australia, pp. 3-36.
- Murzyn, F., and Chanson, H. (2009). Free-surface fluctuations in hydraulic jumps: Experimental observations. *Experimental Thermal and Fluid Science*, Vol. 33, No. 7, pp. 1055-1064 (DOI: 10.1016/j.expthermflusci.2009.06.003).
- Rajaratnam, N. (1967). Hydraulic Jumps. *Advances in Hydrosience*, Ed. V.T. Chow, Academic Press, New York, USA, Vol. 4, pp. 197-280.